ELSEVIER

Evaluation of residual stresses in a SOFC stack

H. Yakabe [a,*], Y. Baba [a], T. Sakurai [a], M. Satoh [b], I. Hirosawa [b], Y. Yoda [b]

[a] *Technical Research Institute, Tokyo Gas Co. Ltd., 16–25 Shibaura, 1-Chome, Minato-ku, Tokyo 105-0023, Japan*
[b] *Japan Synchrotron Radiation Research Institute, Sayo-gun Hyogo, 1-1-1 Kouto, Mikazuki-cho 679-5198, Japan*

Abstract

Residual stresses in a stack of the anode-supported planar SOFC were measured by the X-ray diffraction method (the $\sin^2\psi$ method). The stack used for the stress measurements was composed of a single cell and separators of an alloy. In this measurement, the residual stresses in the electrolyte under the alloy separator and the cathode were focused on. In order to detect the diffraction from the electrolyte under the separator or the cathode, an X-ray energy of 38.8 keV was selected. For the stress measurement, a diffraction peak of YSZ(7 1 1) plane was used. A synchrotron radiation was employed as an excellent X-ray radiation for precise stress measurements. In addition to the stress measurements, numerical simulations for the residual stresses in the cell stack were carried out.
© 2004 Elsevier B.V. All rights reserved.

1. Introduction

Anode-supported cells are inherently strong against stresses because the electrolyte hardly suffers a tensile stress. For cell stacks, certain alloys can be used as interconnectors and auxiliary components of cell stacks, and thus, using the flexibility of the alloys, it is possible to make the cell stack robust against a mechanical load [1,2]. On the other hand, regarding thermal stresses, great care should be taken into account, since the thermal expansion behavior is different between the cell and the alloys. The thermal stress induces a deformation of the cell stack, and sometimes, the cell stack is destroy. To reduce the thermal stress in the cell stack, the metal alloys have to be selected carefully so that the thermal expansion coefficients (TEC) would match well with that of the cell. To study the best alloy as the stack component, we simulated the residual stresses in the cell stack with alloys of various TEC. However, it was difficult to calculate the residual stress in the cell components with a high accuracy since there were many uncertain parameters in the stress calculation (e.g. a temperature at which the cell components are constrained each other, or effect of the reduction of the anode on the stress). To evaluate the residual stress in the cell components precisely by the numerical calculation, it is indispensable to measure the residual stresses practically, and fix these uncertain parameters.

The X-ray stress measurement is an effective method to measure the residual stress in materials without destruction [3–6]. We applied the method to measure the residual stresses in the cell stack. A synchrotron radiation was used as an excellent X-ray radiation for precise stress measurements. Residual stresses in the electrolyte of the cell stack used for practical measurements of the stack performance were measured directly using the X-ray. In addition to the naked electrolyte, the stresses in the electrolyte under the cathode or the alloy were measured. Numerical calculations on the residual stresses in the cell stack were also carried out, and the experimental and numerical results were compared.

2. Experimental

Anode-supported cells were fabricated by a co-firing process. Details of the cell fabrication have been reported elsewhere [7]. For the cell stack, electrically conductive or insulating alloys were applied to the interconnectors and separators, respectively. Fig. 1 shows the cross-sectional diagram for a single-cell stack. A cell was supported using a thin alloy foil, and the alloy foil was sandwiched by alloy frames. A glass sealant was used to connect the cell and the foil, or the foil and the frame. The alloy foil has a role to separate the fuel and air. Metal interconnectors as current correctors were set at the upper and the lower side of the cell, but they are not drawn in the figure.

* Corresponding author. Fax: +81-3-3453-7583.
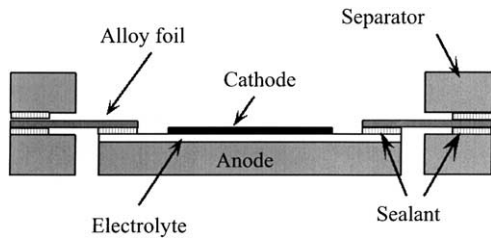*E-mail address:* yakabe@tokyo.co.jp (H. Yakabe).

Fig. 1. Cross-sectional view of the one-cell stack.

The residual stress measurements were carried out using the single-cell stack. The cell stack has already been tested its performance at 750 °C in an electrical furnace. The used stack was directly mounted on the sample stage at the synchrotron facility as shown in Fig. 2 and the residual stresses of the cell stack were measured. Fig. 3 shows the image photo of the single-cell stack. The center black square is a cathode, and around the cathode, the naked electrolyte exists. The edge part of the electrolyte is covered by the alloy
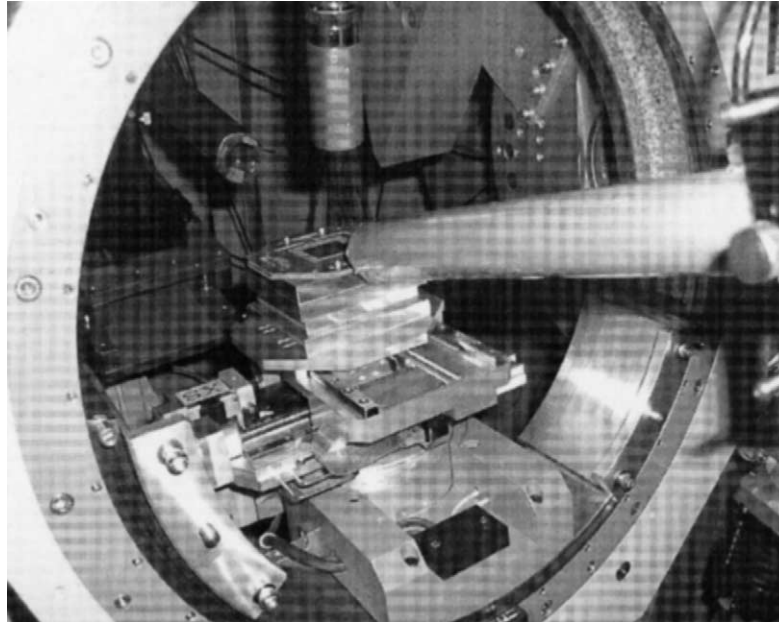

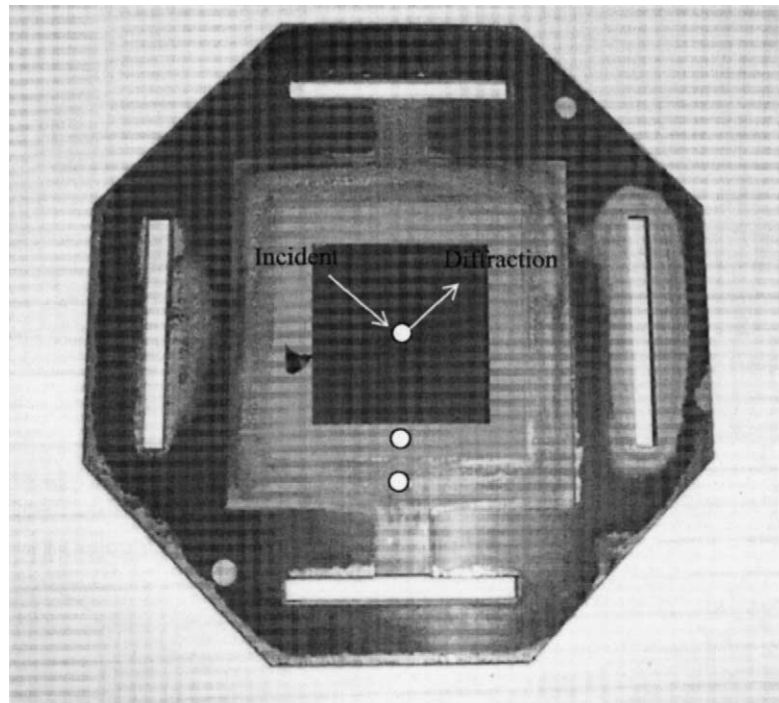Fig. 2. Photo image of the experimental stage at BL19B2 line.

Fig. 3. Photo image of the one-cell stack. The incident beam was irradiated to the three points indicated by filled circles.

foil, and the foil was supported by the separator frame. In this stress measurement, we focused on the residual stresses in the electrolyte of the cell stack at three different points. The three measuring points are pointed by white circles in the figure. One stress focused was that at the naked electrolyte, and the others were the stresses in the electrolytes under the cathode, or the alloy foil. Although the residual stress at the naked electrolyte can be measured easily, it is difficult to measure the residual stresses in the electrolyte under the cathode, or the alloy foil. To measure the residual stress in the electrolyte under the cathode, or the alloy foil, it is necessary to detect the diffraction of the X-ray from the electrolyte through the cathode or the alloy foil. Hence, it was important to select an appropriate X-ray energy which enables us to detect the diffraction from the electrolyte under the cathode or the alloy. Thicknesses of the cathode and the foil were 30 and 50 μm, respectively, and, the shortest beam path in the alloy was 100 μm even when the beam was irradiated in the perpendicular direction to the cell surface. The main element of the alloy was α-Fe, and the attenuation length of the X-ray in the iron is displayed in Fig. 4. The X-ray energy of more than 30 keV is required to obtain the attenuation length of 100 μm in α-Fe. Thus, we selected the X-ray energy of 38.7 keV for the stress measurement.

A synchrotron radiation was employed as the X-ray source. The synchrotron radiation is an ultra-bright, highly directional, and collimated light. In addition, wide spectrum of wavelengths, stretching from infrared to X-rays can be used. For the present stress measurement, an X-ray beam with a high energy and a high brightness are necessary, and thus, the synchrotron radiation is the best source for the present purpose.

The experiment was performed at BL19B2 line at SPring-8, which is a medium-length hard X-ray bending magnet designed for the purpose of engineering science researches. The Huber multi-axis diffractometer composed

Table 1
List of the stress measuring conditions

X-ray source	Bending magnet
X-ray energy	38.7 keV
Monochrometer	Si311
Measuring method	Side-inclination

of conventional four circle goniometer and additional four axes was mounted at BL19B2, which was suited for the present stress measurement.

Table 1 shows a list of the conditions for the stress measurements. As mentioned above, the X-ray energy was set to 38.7 keV, which was enough to detect the diffraction beam from the electrolyte through the alloy foil or the cathode. Fig. 5 displays the result of θ–2θ scan for the electrolyte of the cell stack. The incident beam was irradiated to the naked electrolyte part. The peaks pointed with asterisks correspond to the cubic YSZ structure, and the other peaks are diffractions from Ni of the Ni/YSZ anode under the electrolyte. For the X-ray stress measurement, in general, a diffraction peak at a high 2θ angle is used because enough large ψ can be used. On the other hand, the intensities of the diffraction peaks at a high 2θ angle are weaker, and, many peaks from different diffracting planes overlap each other. Thus an optimal diffracting plane has to be selected for the stress measurement. We searched a single diffraction peak existing at a higher angle and having enough intensity for the stress measurement, and selected the peak of YSZ(7 1 1) plane. As one can see in Fig. 5, the peak center of YSZ(7 1 1) peak is around 25.7°. If the iso-inclination method is employed, available maximum ψ becomes <13°, which is not enough to obtain accurate analyses. To obtain an enough high tilting angle ψ, we employed side-inclination method instead of the iso-inclination method. Regarding side-inclination method, the footprint of the beam at the surface of the sample at a
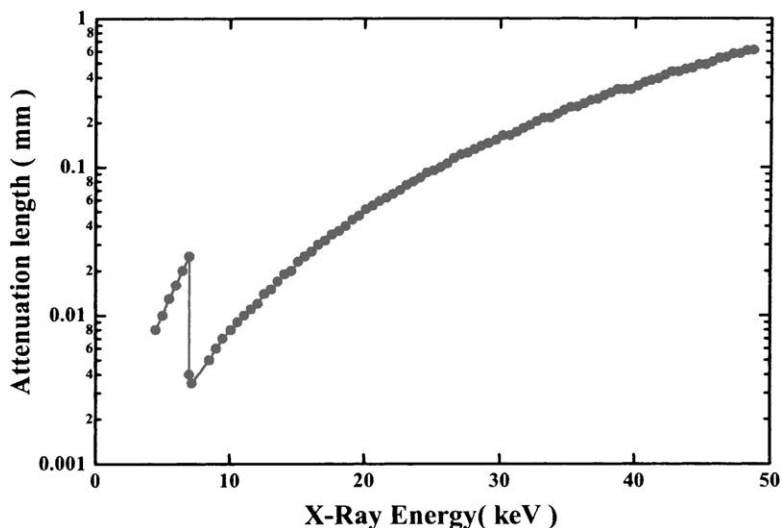

Fig. 4. Attenuation length of the X-ray inside iron when the direction of the incident beam is perpendicular to the sample surface.
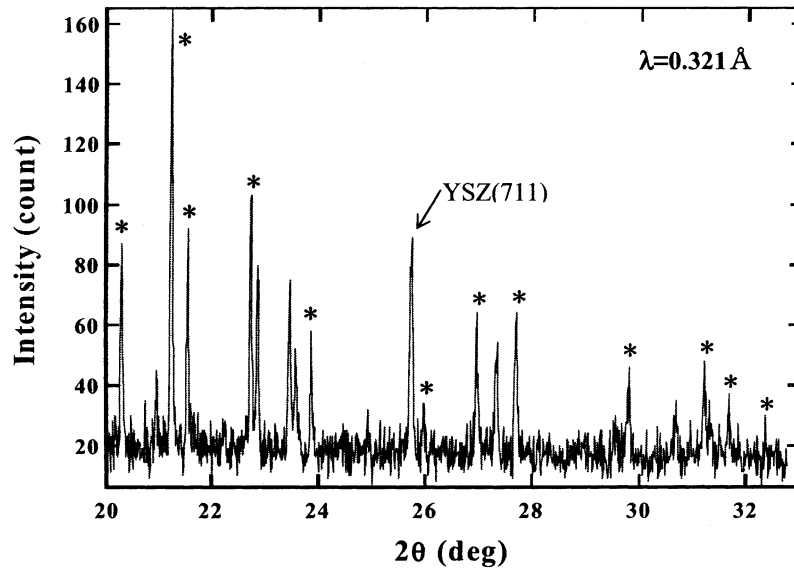
Fig. 5. X-ray diffraction pattern for the electrolyte of the anode-supported cell.

3. Results and discussion

Fig. 6 shows the result of a θ–2θ scan where the incident beam was irradiated to the foil part. One can see that the YSZ(7 1 1) peak appears in the chart, indicating that the diffraction from the electrolyte through the alloy foil could be detected. Fig. 7(a)–(c) display the shift of the YSZ(7 1 1) peak with ψ. The incident beam was irradiated to the naked electrolyte, the cathode part, and the alloy foil for cases (a)–(c), respectively. For all the cases, the YSZ(7 1 1) peak shifts toward higher angle with increasing ψ. Only for case (c), can one see the split of the YSZ(7 1 1) peak. We consider that the split may come from an imperfect control of the incident beam size (i.e. the beam spot may slightly spread to the naked electrolyte part). The peak profiles obtained were fitted using the Gaussian function as shown in Fig. 8, and the peak centers were determined. Fig. 9(a)–(c) show the d–$\sin^2\psi$ diagrams estimated using the detected YSZ(7 1 1) diffraction peak. Although the scattering of the plot is larger for case (c), d decreases linearly with $\sin^2\psi$ for all the cases.
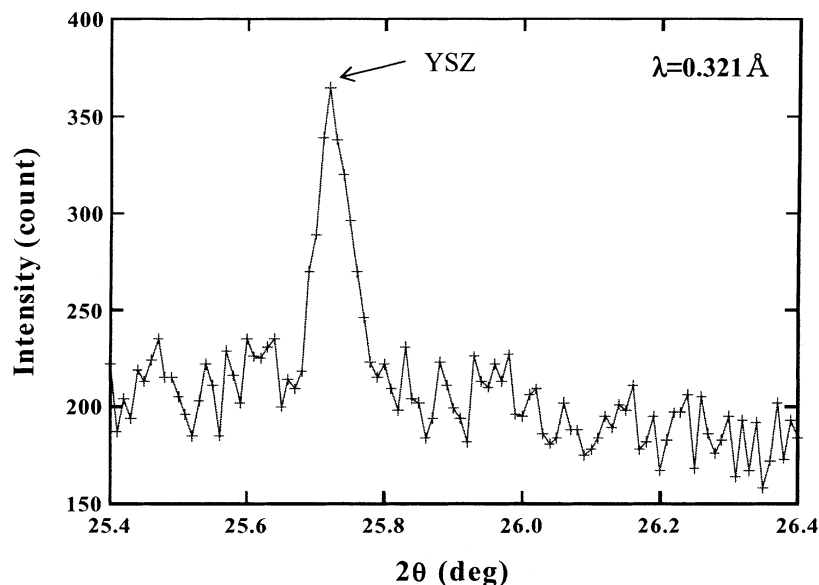
large ψ becomes large. The size of the incident beam at the sample surface was controlled with a Ta-blade slit so that the incident beam would be irradiated to within the targeted area.

Fig. 6. Result chart of θ–2θ scan. The incident beam was irradiated to the foil part.
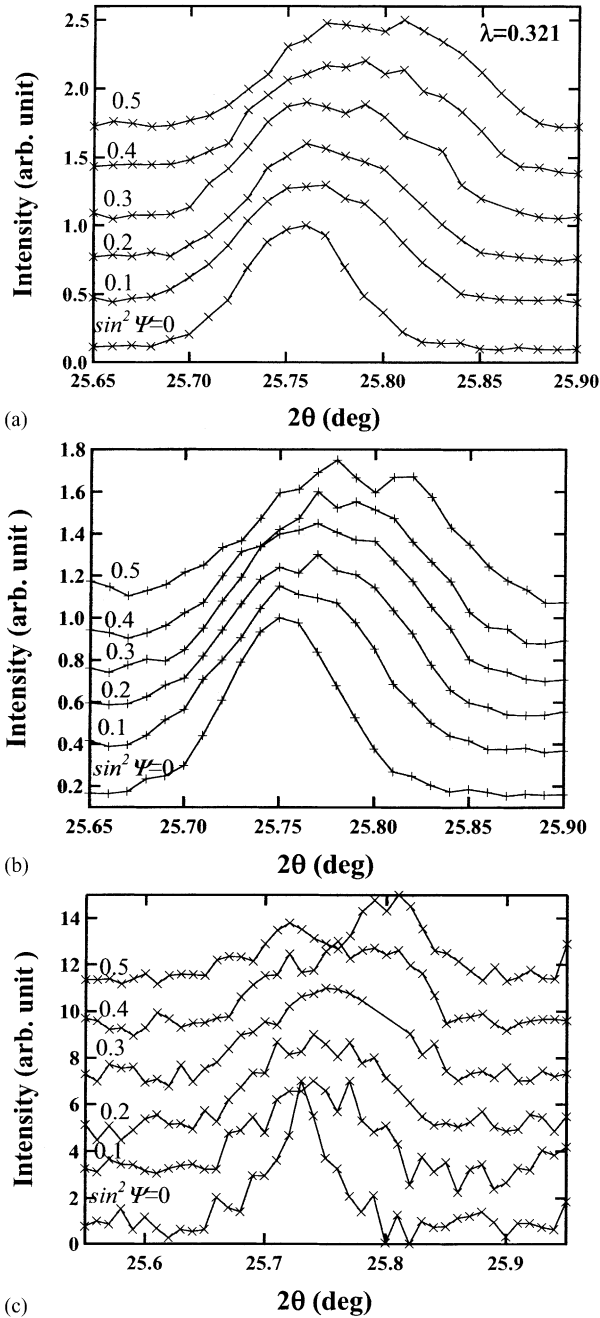
(a)

(b)

(c)

Fig. 7. Results of 2θ scan for different ψ. The incident beam was irradiated to: (a) the naked electrolyte part of the foil part; (b) the cathode part; and (c) the alloy foil part.

Thus, we can estimate the residual stresses in the electrolyte using the following formula.

$$\sigma = \frac{E}{1 + \upsilon} \times \frac{1}{d_0} \times \frac{\partial d}{\partial \sin^2 \psi} \qquad (1)$$

where d_0 is the interplanar spacing under a stress-free condition, E and υ are the elastic constant and Poisson's ratio. In the X-ray stress measurement, E and υ must be measured using the X-ray method. In the present stress measurement, however, we did not measure the X-ray elastic constants.

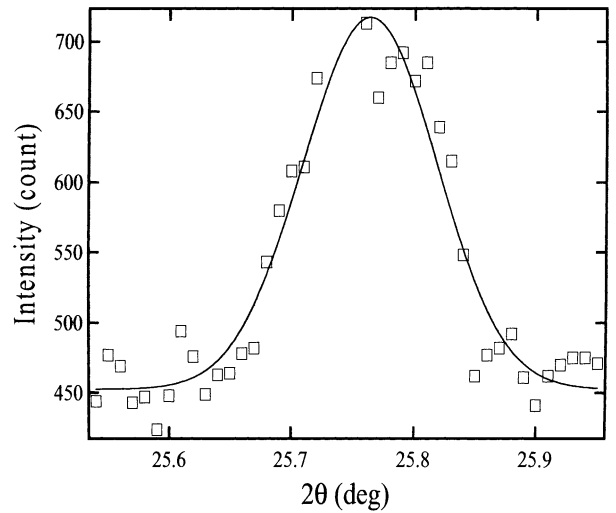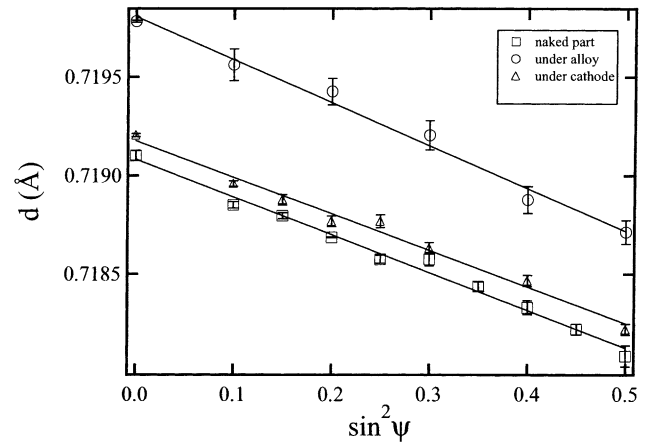Fig. 8. Fitting for the obtained peak profiles in Fig. 7(c) using the Gaussian function.

Fig. 9. The d–$\sin^2 \psi$ diagram measured for the single stack: open squares, open circles, and open triangles are for the naked electrolyte, the electrolyte under the cathode, and the electrolyte under the alloy foil, respectively.

Thus we employed the calculated value of the elastic constants for the stress estimation (they are listed in Table 2). These elastic constants were calculated from the reported elastic constants of cubic YSZ [4,8] using the Voight model [9]. In the Voight model, the elastic constant is independent of the diffracting plane. The estimated residual stresses in the electrolyte using the calculated elastic constants are

Table 2
List of the stiffness of the cubic YSZ used for the calculation of the elastic constant

Elastic constant	Electrolyte (GPa)
C_{11}	400
C_{12}	110
C_{44}	55
$E/(1 + \upsilon)$	182

Table 3
List of the estimated residual stresses in the electrolyte

Part	Evaluated stress (MPa)
At naked electrolyte	486
Under cathode	471
Under alloy	551

listed in Table 3. Everywhere in the electrolyte, the estimated residual stresses were compressive stresses. As compared to in the naked electrolyte, the calculated residual stress is slightly small under the cathode, and large under the alloy foil. Thus, it was found that stacking the cell changes the residual stress in the electrolyte.

In addition to the stress measurements, the distributions of the residual stresses in the stack were simulated using a computer simulation technique. The stack geometry (cathode–electrolyte–anode, separator, and frame) was modeled precisely, and the distributions of the residual stresses in the stack components were calculated using the finite element method (details of the method for the stress simulation have been reported previously [10]). In the present simulation, we assumed several calculating conditions. First assumption was the temperature at which the stack components were constrained (connecting temperature). The temperatures at which the electrolyte and the anode, the electrolyte and the cathode, and the electrolyte and the alloy foil are connected were assumed to be 1400, 1250, and 900 °C, respectively. In the simulation, above 1400, 1250, and 900 °C, the anode, the cathode, and the glass sealant were treated as plastic materials. That is, only below the connecting temperature, these components would contribute to the residual stress in the electrolyte. Second assumption was that the reduction of the anode (i.e. the change of NiO to Ni in the anode) would not affect the residual stress in the electrolyte. Our previous stress measurements for the co-fired cells revealed that there was no marked difference in the residual stresses between the cells with the oxidized and the reduced anodes [10].

Fig. 10(a) displays the simulated stress distribution in the electrolyte at room temperature. The absolute value of the residual stress is smaller under the cathode and larger under the alloy foil than in the naked electrolyte, which is qualitatively consistent with the result of the stress measurements. The comparison of the residual stresses for the measured and simulate values are listed in Table 4. As compared to the simulated values, the measured values are larger by

Table 4
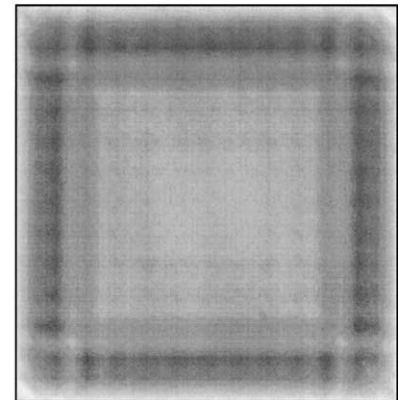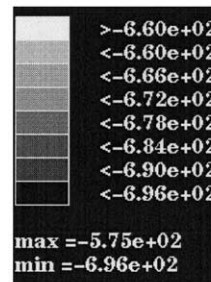Comparison of the measured and simulated stresses

Part	Measured stress (MPa)	Simulated stress (MPa)	Modified measured stress (MPa)
At naked electrolyte	486	679	633
Under cathode	471	670	612
Under alloy	551	705	719
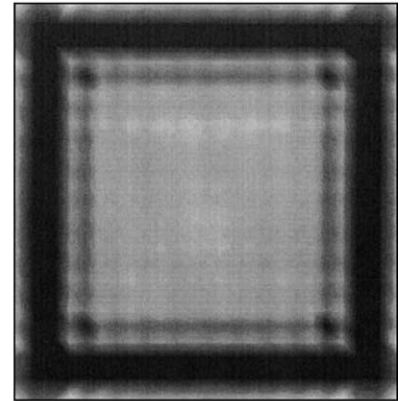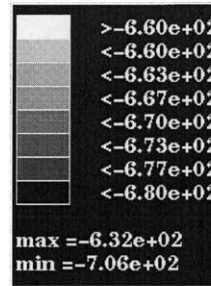
Fig. 10. Simulated distribution of the residual stress in the electrolyte at room temperature: (a) for the single stack; and (b) for the single cell.

20–30%. This discrepancy may originate from the following two reasons. One is the connecting temperatures were not proper in the stress simulation. If the actual connecting temperature is lower than we assumed it to be, the simulated values become larger than the measured values. Another reason is that the elastic constants used for the stress estimation were inadequate. Since the X-ray elastic constants, in general, depend on the diffracting plane, also in the present stress measurement, the X-ray elastic constants must be measured using the YSZ(7 1 1) peak. However, we used the calculated values as the elastic constant, and thus it may result in a less estimation of the residual stresses. Fig. 10(a) and (b) are the comparison of the simulated residual stresses in the electrolytes for the single cell and the single stack. From the figures, we can find that the residual stress at the naked electrolyte for the stack model is almost the same as that at the center for the single cell. This suggests that the stacking of the cell will not affect the residual stress at the naked electrolyte. In our previous evaluation of the residual stress for the single cell, the measured stress and the simulated stress in the electrolyte were almost the same. In the previous evaluation, the same X-ray elastic constants as the present estimation were employed to estimate the residual stress. Besides, in the previous stress calculation, the connecting temperature between the electrolyte and the anode

was assumed to be 1400 °C which is the same as the present assumed values. Considering these facts, we can conclude that the origin of the discrepancy between the measured and the calculated stresses in the present case is improper elastic constants.

As mentioned above, for the stress simulation, the residual stress at the naked electrolyte of the stack is almost the same as that at the center of the single cell. Accordingly, we assume that the residual stress in the naked electrolyte of the stack is the same as that at the center part of the electrolyte for the single cell, and modify the elastic constants. Table 4 shows the modified residual stresses in the electrolyte assuming that the stress at the naked electrolyte is the same as that of the single cell. The modified and simulated residual stresses become close. For more accurate experimental estimations, the X-ray elastic constant must be measured using the YSZ(7 1 1) peak.

The strength of YSZ against the compressive stress is more than 1 GPa [11] and thus these residual stresses are not so large as to induce a failure of the electrolyte.

4. Conclusion

The residual stresses in the electrolyte of the single-cell stack were evaluated using experimental and numerical methods. The estimated stresses in the electrolyte were compressive stresses of 633, 612 and 719 MPa at the naked part, under the cathode, and under the alloy foil, respectively. Although the stacking of the cell slightly increases the residual stress in the electrolyte under the alloy foil, the residual stresses are not so large as to induce a failure of the electrolyte.

References

[1] Y. Baba, T. Ogiwara, H. Yakabe, Y. Matsuzaki, Abstracts of 2002 Fuel Cell Seminar, 2002, p. 340.
[2] J. Zizelman, S. Mukerjee, Abstracts of 2002 Fuel Cell Seminar, 2002, p. 842.
[3] I.C. Noyan, J.B. Cohen, Adv. X-ray Anal. 27 (1984) 129.
[4] K. Tanaka, Y. Yamamori, N. Mine, K. Suzuki, in: Proceedings of the 32nd Japan Congress on Materials Research, vol. 199, 1989.
[5] Y. Yoshioka, Adv. X-ray Anal. 24 (1981) 167.
[6] M. Barral, J.M. Sprauel, J. Lebrun, G. Maeder, S. Megtert, Adv. X-ray Anal. 27 (1984) 149.
[7] I. Yasuda, Y. Baba, T. Ogiwara, H. Yakabe, Y. Matsuzaki, Proc. Solid Oxide Fuel Cells VII (2001) 131.
[8] B.J. Botha, J.C.H. Chiang, P.M. Mjawara, P.E. Ngoepe, J. Appl. Phys. 73 (11) (1993) 7268.
[9] W. Voight, "Lehrbuch der Kristallphysik", Tebubner, Berlin, 1928, p. 962.
[10] H. Yakabe, M. Hishinuma, M. Uratani, Y. Matsuzaki, I. Yasuda, J. Power Sources, in press.
[11] T. Kato, N.S. Wang, A. Negishi, A. Momma, Y. Kasuga, K. Nozaki, in: Proceedings of the Third International Fuel Cell Conference, Nagoya, 3 November, 1999, p. 461.